JACS
JOURNAL OF THE AMERICAN CHEMICAL SOCIETY

COMMUNICATION

pubs.acs.org/JACS

Protein−Ligand Structure and Electronic Coupling of Photoinduced Charge-Separated State: 9,10-Anthraquinone-1-sulfonate Bound to Human Serum Albumin

Yasuhiro Kobori*[,†,‡] and Masaaki Fuki[†]

[†]Department of Chemistry, Faculty of Science, Shizuoka University, 836 Ohya Suruga-ku, Shizuoka 422-8529, Japan

[‡]PRESTO, Japan Science and Technology Agency, 4-1-8 Honcho Kawaguchi-shi, Saitama 332-0012, Japan

Supporting Information

ABSTRACT: To elucidate how the protein−ligand docking structure affects electronic interactions in the electron-transfer process, we have analyzed time-resolved electron paramagnetic resonance spectra of photoinduced charge-separated (CS) states generated by light excitation of 9,10-anthraquinone-1-sulfonate ($AQ1S^-$) bound to human serum albumin at a hydrophobic drug-binding region. The spectra have been explained in terms of the triplet−triplet electron spin polarization transfer model to determine both the geometries and the exchange couplings of the CS states of $AQ1S^{2-\bullet}$−histidine-242 radical cation ($H242^{+\bullet}$) and $AQ1S^{2-\bullet}$−tryptophan-214 radical cation ($W214^{+\bullet}$). For the CS state of the former, it has been revealed that, due to the orthogonal relationship between the singly occupied molecular orbitals of $AQ1S^{2-\bullet}$ and $H242^{+\bullet}$, the electronic coupling (5.4 cm^{-1}) is very weak, contributing to the prevention of energy-wasting charge recombination, even at a contact edge-to-edge separation.

Analysis of the effect of the molecular geometry on the electronic interaction between a ligand and its target protein is crucial to directly understand how protein structures play key roles in several biological processes.[1−12] As an example, in DNA photolyases, radical pairs (RPs) composed of bound cofactor radicals and tryptophan radicals are generated upon photoactivation of the enzymes by photoinduced electron transfer (ET) through the cofactor−tryptophan electronic interactions.[3,6,12,13] Moreover, the protein−ligand structure of the photoinduced charge-separated (CS) state should be essential in the artificial design of useful functions for biological solar-energy conversion and for biophotocatalysis.[7,14−17] Many studies have been performed to determine the electronic coupling (V_{DA}) between the electron donors and acceptors in protein systems.[4,5,7−10,18] Using quantum mechanical theories, the effects of molecular geometry on V_{DA} have been predicted through several mediators in terms of the superexchange mechanism.[4,9,10,18−20] Despite the importance of understanding the electronic interactions, no study has experimentally clarified both the 3D structure and the V_{DA} in photoinduced, protein−ligand CS state systems.

In the present study, we employ human serum albumin (HSA) as a model protein to elucidate the effect of geometry on V_{DA} in a protein−ligand system. 9,10-Anthraquinone-1-sulfonate ($AQ1S^-$) is employed as the ligand.

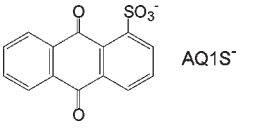

Since 9,10-anthraquinone disulfonate has been shown to bind to a hydrophobic site in subdomain IIA, to which an aromatic anion of the drug warfarin binds,[21] $AQ1S^-$ is expected to bind to the same region. We characterized a protein−ligand geometry of the photoinduced CS state in which charge recombination (CR) is electronically prohibited, even though a radical cation of histidine and a radical anion of the ligand are in close proximity at the drug-binding region. This unique RP state has been revealed using time-resolved electron paramagnetic resonance (TREPR) measurements at a low temperature. We recently proposed a model of triplet−triplet electron spin polarization transfer (ESPT) by which the anisotropic magnetic properties of the excited triplet states are transferred to the CS states that are detected by TREPR.[22] This model is applied to determine the protein−ligand docking structure and the V_{DA} in the transient CS states.

Figure 1a shows the TREPR spectrum obtained 1 μs after depolarized 355 nm laser irradiation of the $AQ1S^-$ (3 mM)−HSA (3 mM) system in frozen aqueous phosphate buffer solution (pH 7.0) at 100 K. The red spectrum is the sum of the blue line and the dotted line components in Figure 1d. The blue spectrum represents the fine structure due to the dipolar interaction between the two electron spins.[23,24] From the entire width of this spectrum, $|D| \approx 10$ mT is estimated as the dipolar splitting constant. By the point-dipole approximation, the distance between the two spins is calculated to be $r_{SS} \approx 0.65$ nm, indicating that a contact RP state is generated in the protein. The blue spectrum in Figure 1d is composed of the net E spin polarization and the E/E/A/A pattern in the fine structure, where A and E denote microwave absorption and emission, respectively. The net E effect is explained by the triplet mechanism (TM)[25] by which the electron spin polarization (ESP), characterized by the population difference between the highest sublevel and the lowest sublevel in the precursor excited triplet state, is transferred to the triplet RP state.[22] Since the highest triplet sublevel is the most populated due to the effective S_1-T_1 intersystem crossing

Received: July 23, 2011
Published: October 05, 2011

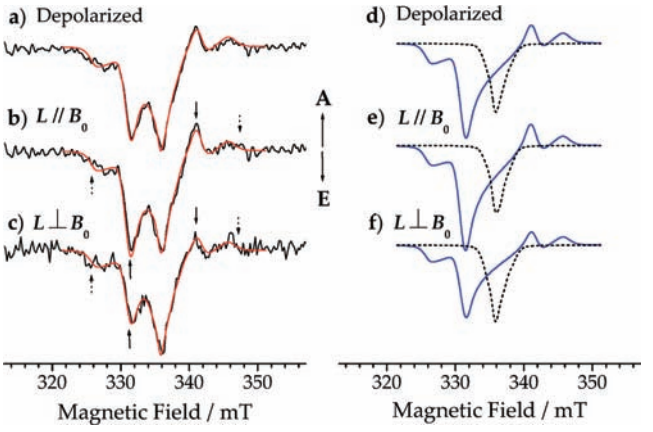

Figure 1. (Left) TREPR spectra (black lines) of the $AQ1S^{-}$−HSA system obtained 1 μs after 355 nm laser excitation at 100 K using (a) depolarized light, (b) light $\boldsymbol{L}$ parallel to the external magnetic field $\boldsymbol{B}_0$, and (c) $\boldsymbol{L}$ perpendicular to $\boldsymbol{B}_0$. (Right) Computed TREPR spectra of the photoinduced CS states composed of $AQ1S^{2-\bullet}$ and $His^{+\bullet}$ (blue solid lines) and of $AQ1S^{2-\bullet}$ and $Trp^{+\bullet}$ (dotted lines), considering (d) depolarized light, (e) $\boldsymbol{L}$ parallel to $\boldsymbol{B}_0$, and (f) $\boldsymbol{L}$ perpendicular to $\boldsymbol{B}_0$. The red spectra superimposed on the experimental data on the left are obtained by summing the corresponding blue solid lines and the dotted lines from the right.

(ISC) to the Z sublevel in the $^3n\pi^*$ configuration of 9,10-anthraquinone (AQ),[26] the net E is explained by a photoreaction between a residue and the excited triplet state of the bound $AQ1S^{-}$.[21] The E/E/A/A pattern in the RP state is also the consequence of the ESPT from the precursor triplet state.[22,24,27−29] $^3AQ^*$ is known to exhibit an E/E/E/A/A/A polarization pattern due to ISC to the Z sublevel.[26] Thus, the observation of E/E/A/A indicates that the direction of the principal Z axis in the RP state is close to the direction of the Z axis in the excited triplet state, as detailed in the Supporting Information (SI).

When the excitation laser light polarization ($\boldsymbol{L}$) is set parallel to the external magnetic field ($\boldsymbol{B}_0$) in Figure 1b, the inner peak intensities, indicated by solid arrows, become stronger than the inner peak intensities in Figure 1a, while the outer peak intensities, indicated by dotted arrows, are almost unchanged. On the other hand, when $\boldsymbol{L}$ is set perpendicular to $\boldsymbol{B}_0$ in Figure 1c, the inner peaks become weaker, as shown by the solid arrows. These laser polarization effects[30] imply that the position and orientation of the RP state are defined with respect to the electronic transition dipole moment of the ligand in the protein matrix.[27] As for the emissive peak at 336 mT in the center of Figure 1a, the signal has a broadness of ∼3 mT; the width of the peak is greater in Figure 1c than in Figure 1b. This laser polarization effect shows that the line shape of the minor center peak also originates from the dipolar interaction ($|D| = 1.7$ mT) of a RP with $r_{SS} \approx 1.2$ nm, generated by the photoreaction between another residue and the triplet $AQ1S^{-}$ bound in the protein. From an X-ray structure of a HSA−warfarin complex (PDB code 2BXD[31]), shown in Figure 2, one can see that a histidine (H242) and a tryptophan (W214) are located near the aromatic anion molecule of warfarin. These residues can be energetically oxidized by $^3AQ1S^{-*}$ to generate the CS states.[32,33] (See SI for details of the energetics.) The center-to-center distances obtained from the X-ray data are 0.63 and 1.22 nm for warfarin−H242 and for warfarin−W214, respectively, indicated by the red and blue arrows in Figure 2.[31] These distances are compatible with the r_{SS} values estimated above.

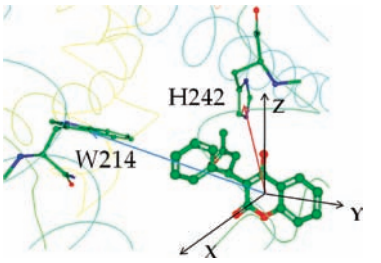

Figure 2. X-ray structure of a warfarin−HSA complex at the binding region, obtained from PDB entry 2BXD. The positions and orientations of W214 and H242 are shown with respect to the axes set in warfarin.

It is therefore concluded that $AQ1S^{-}$ is bound to the warfarin-binding region to generate the photoinduced CS states of $AQ1S^{2-\bullet}$−$H242^{+\bullet}$ and $AQ1S^{2-\bullet}$−$W214^{+\bullet}$. The two different CS species originate from the excited states of $AQ1S^{-}$ located in the same area in the protein matrix. Based on the signal intensities, the two CS states are generated with roughly equal populations, indicating that the CS rate constants are of the same order of magnitude. This result is reasonably explained by the ET theory using the appropriate V_{DA} values (vide infra) and the driving forces, as detailed in the SI.

To analyze the geometries and exchange couplings ($2J$) of the RP states, we applied the ESPT model recently developed for the spin-correlated RP (SCRP) generated by the triplet-precursor reaction.[22] In the SCRP levels, we considered the anisotropic hyperfine couplings and $\mathbf{g}$-tensors in the RP states of $AQ1S^{2-\bullet}$−$H242^{+\bullet}$ and $AQ1S^{2-\bullet}$−$W214^{+\bullet}$. We also considered the magnetophotoselection effects[30] by which the $\boldsymbol{B}_0$ directions in the precursor triplet states and the RP states are distributed with respect to the electronic transition dipole moment of $AQ1S^{-}$. (See SI for the theory and details of the EPR parameters employed.) To calculate spin polarization via the ESPT in the presence of an external magnetic field, the sublevel populations are first calculated for the excited triplet $AQ1S^{-}$ using the dipolar splitting parameters[35] $D_T = -237$ mT and $E_T = 5.3$ mT, taking into account the $^3n\pi^*$ configuration reported for AQ in a nonpolar matrix.[26] Sublevel-selecting ratios for the S_1-T_1 ISC are considered to be $p_X = p_Y = 0$ and $p_Z = 1$ for the T_X, T_Y, and T_Z levels, respectively, due to the spin−orbit coupling between $^1\pi\pi^*$ and $^3n\pi^*$.[35] $D = -10.4$ and -1.7 mT are employed for $AQ1S^{2-\bullet}$−$H242^{+\bullet}$ and for $AQ1S^{2-\bullet}$−$W214^{+\bullet}$, respectively, with $E = 0.0$ mT, where E is the dipolar coupling parameter corresponding to the spin-density distribution difference between the X' and Y' directions, both of which are perpendicular to the principal Z' axis.[35] The Z' axes of the dipolar interactions in the CS states are represented by the red and blue arrows in Figure 3a, using the polar angles (θ,ϕ) with respect to the principal axes (X, Y, and Z) of the dipolar interaction of the $^3n\pi^*$ state in $AQ1S^{-}$. In the ESPT calculation, we apply the slow reaction model so that the oscillatory coherence terms in the excited triplet state are not transferred to the CS state.[22] This is because the net TM effect is generated by the effective averaging of triplet coherences while the CS reaction proceeds.[22] As reported previously, we consider that the CS state undergoes $S-T_0$ mixing to create the spin-correlated RP levels[11,36,37] by interactions of J, D, and the hyperfine couplings in the RP state.[22]

The calculated laser polarization effects on the TREPR signals are shown on the right side of Figure 1 for $AQ1S^{2-\bullet}$−$H242^{+\bullet}$ (blue lines) and $AQ1S^{2-\bullet}$−$W214^{+\bullet}$ (dotted lines). The red spectra,

dx.doi.org/10.1021/ja206898j |J. Am. Chem. Soc. 2011, 133, 16770–16773

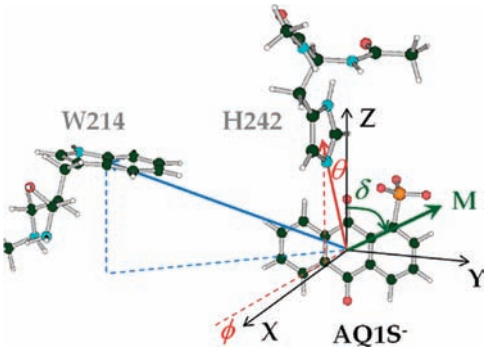

Figure 3. EPR geometries of the photoinduced CS states of $AQ1S^{2-\bullet}$−$H242^{+\bullet}$ and $AQ1S^{2-\bullet}$−$W214^{+\bullet}$ with respect to the molecular axes (*X*, *Y*, and *Z*) of the spin dipolar interaction of $^3AQ1S^{-}$*. $(\theta,\phi) = (8°,-9°)$ and $(54°,-65°)$ are obtained as the directions of the principal axes of *Z*′ in $AQ1S^{2-\bullet}$−$H242^{+\bullet}$ and $AQ1S^{2-\bullet}$−$W214^{+\bullet}$, respectively, by the simulations in Figure 1 using the triplet ESPT model. The direction of the transition dipole moment (**M**) of $AQ1S^{-}$ is determined to be $\delta = 51°$.

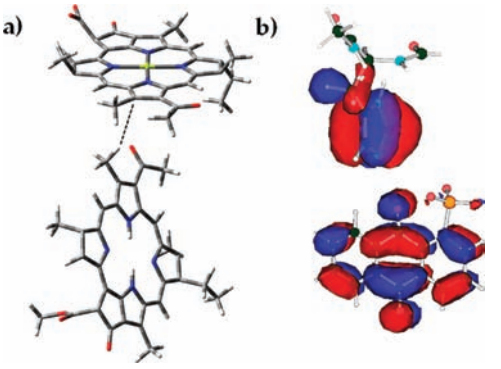

Figure 4. Comparison of the electron-transfer geometries between (a) $BCh^{-\bullet}$−BPheo in *Rhodobacter sphaeroides* (PDB code 1Z9K[34]) and (b) the photoinduced CS states of $AQ1S^{2-\bullet}$−$H242^{+\bullet}$ in Figure 3. The direct overlap (dashed line) between the π-orbital in BChl and the C−H σ^*-orbital in the methyl group in BPheo contributes to the large electronic coupling ($|V_{DA}| \approx 60\ cm^{-1}$) for the ET in (a). The unpaired electronic orbitals are shown on $AQ1S^{2-\bullet}$−$H242^{+\bullet}$ in (b), representing the weak electronic coupling ($|V| = 5.4\ cm^{-1}$) for CR due to the orthogonal orbital relationship.

obtained by summing the corresponding blue and dotted lines, well reproduce the experiments in Figure 1. The angle parameters of the CS states are $(\theta,\phi) = (8°,-9°)$ for $AQ1S^{2-\bullet}$−$H242^{+\bullet}$ and $(54°,-65°)$ for $AQ1S^{2-\bullet}$−$W214^{+\bullet}$. Moreover, the transition dipole moment (**M**) upon 355 nm excitation in $AQ1S^{-}$ is determined to be $\delta = 51°$ when **M** is set to lie in the *YZ* plane, as shown by a green arrow in Figure 3. $\delta = 51°$ is consistent with the singlet π−π^* transition of $AQ1S^{-}$ around 355 nm, as estimated by time-dependent density functional theory molecular orbital calculations. (See the SI.) The molecular geometries in Figure 2 are coincident with the X-ray structure of the HSA−warfarin complex; when we set the *Z* axis parallel to the C−O direction and the *X* axis perpendicular to the aromatic plane of warfarin, as shown in Figure 2, $(\theta,\phi) = (19°,0°)$ for warfarin−H242 and $(52°,-61°)$ for warfarin−W214 are obtained from 2BXD[31] and are sufficiently close to the geometries determined in the present systems. Inclusion of the positive exchange couplings ($2J$) as the S−T energy gaps in the SCRPs is essential to fully reproduce the spectra. $2J$ = 4.1 and 0.2 mT have been determined for the contact CS state ($AQ1S^{2-\bullet}$−$H242^{+\bullet}$) and for the distant CS state ($AQ1S^{2-\bullet}$−$W214^{+\bullet}$), respectively. The positive $2J$ values are explained by the CT interaction (J_{CT}), as has been reported in numerous CS systems.[28,38−41] According to the model of J_{CT}, the exchange coupling is approximated as $2J_{CT} = |V|^2/\Delta E_{CR}$, where $|V|$ and ΔE_{CR} are the electronic coupling matrix element and the vertical energy gap for the CR, respectively.[24,39] Thus, in the CS state of $AQ1S^{2-\bullet}$−$H242^{+\bullet}$, $|V| = 5.4\ cm^{-1}$ is determined from $2J$ = 4.1 mT and from ΔE_{CR} = 1.0 eV, as detailed in the SI. In bacterial photosynthetic reaction centers,[20,42,43] stronger couplings of $|V_{DA}| \approx 60\ cm^{-1}$ are known for ET from the bacteriochlorophyll (BChl) radical anion to bacteriopheophytin (BPheo) at edge-to-edge distances (r_{ee}) of 0.30 nm between the methyl group of BPheo and BChl, as shown by a dashed line in Figure 4a, while r_{ee} = 0.30 nm as well for warfarin−H242 in Figure 2. In the BChl−BPheo systems, SAC-CI theoretical studies[18,20] suggested that electronic interactions between the π-systems and methyl groups have an important effect on the ETs; the direct orbital overlap between the SOMO of the BChl radical anion and the C−H σ^*-orbital in the methyl group in Figure 4a contributes significantly to $|V|$, since the σ^*-orbitals in BPheo are allowed to possess a certain electron density in the LUMO level by hyperconjugation[18] with the π-system of BPheo in *Rhodobacter sphaeroides*. On the other hand, in the present system, such a hyperconjugation effect will not occur since there is no methyl group to directly mediate the electronic coupling in the RP state, as shown in Figure 3. Also, since the warfarin-binding region is known to be hydrophobic[44] in Figure 2, no water molecules are expected to participate in mediating the electronic coupling of the contact CS state.[9] The substantially weaker electronic coupling, even at the contact distance in $AQ1S^{2-\bullet}$−$H242^{+\bullet}$, thus strongly indicates that direct overlap between active SOMOs is highly inhibited by the orthogonal relationship between the π-orbitals, as shown in Figure 4b. This orthogonal orbital conformation is strongly supported by the dipolar coupling parameter of E = 0.0 mT employed for simulations of the contact RP state in Figure 1.[29] $E = 0$ implies that there is no difference in the spin-density distributions between the *X*′ and *Y*′ directions perpendicular to the principal *Z*′ axis, represented by the red arrow in the CS state in Figure 3. Thus, E = 0.0 mT is well compatible with the orbital distribution displayed in Figure 4b, since the spin densities are distributed at the in-plane positions of the aromatic planes in both $AQ1S^{2-\bullet}$ and in $H242^{+\bullet}$. The orthogonal relationship is in line with the structure of the HSA−warfarin complex, since the aromatic plane of H242 is almost perpendicular to the *YZ* plane in warfarin, as revealed by the X-ray structure[31] in Figure 2. Also, the magnitude of $|V| = 5.4\ cm^{-1}$ determined in the present system is quite close to the computed electronic coupling of $<7\ cm^{-1}$ at the direct contact region with the orthogonal porphyrin−porphyrin geometry produced by a protein−protein interaction of bovine cytochrome b5, as reported by Lin et al.[9] The lifetime of the TREPR signal of $AQ1S^{2-\bullet}$−$H242^{+\bullet}$ is determined to be 2 μs, indicating that the CR process is highly prohibited, as detailed in the SI. The above results are all compatible with the orthogonal orbital conformation contributing to the weak electronic interaction for the CR.[24,45]

In conclusion, by means of low-temperature TREPR, we have characterized both the 3D-docking structures and the electronic coupling of protein−ligand CS states. It has been revealed that, due to the orthogonal relationship between the SOMOs in the CS state of $AQ1S^{2-\bullet}$−$H242^{+\bullet}$, the magnitude of the electronic

coupling is <10 cm^{-1}, contributing to the prevention of energy-wasting charge recombination, even at the contact separation. Understanding the geometry effects on the electronic interactions between the ligands and their neighboring residues is quite important in analyzing the pathways for tunneling and transport of electrons and holes in proteins.[7,9,14,15] The present study has demonstrated that TREPR is a powerful tool to experimentally elucidate the underlying biological functions for the CSs, thereby contributing to the development of efficient solar-energy conversions and solar-energy storage devices using biological molecules, including human proteins.

■ ASSOCIATED CONTENT

Supporting Information. Experimental details, optical spectroscopic data, computation methods, and kinetic analyses. This material is available free of charge via the Internet http://pubs.acs.org.

■ AUTHOR INFORMATION

Corresponding Author
sykobor@ipc.shizuoka.ac.jp

■ ACKNOWLEDGMENT

The authors thank Prof. Hisao Murai (Shizuoka University) and Dr. Kiminori Maeda (University of Oxford) for useful discussions. This work was supported by a Grant-in-Aid for Scientific Research (No. 22550009) from Ministry of Education, Culture, Sports, Science and Technology, Japan. This research was partially carried out by using an instrument at the Center for Instrumental Analysis of Shizuoka University.

■ REFERENCES

(1) Xiong, P.; Nocek, J. M.; Vura-Weis, J.; Lockard, J. V.; Wasielewski, M. R.; Hoffman, B. M. *Science* **2010**, *330*, 1075–1078.
(2) Efimova, O.; Hore, P. J. *Biophys. J.* **2008**, *94*, 1565–1574.
(3) Brosi, R.; Illarionov, B.; Mathes, T.; Fischer, M.; Joshi, M.; Bacher, A.; Hegemann, P.; Bittl, R.; Weber, S.; Schleicher, E. *J. Am. Chem. Soc.* **2010**, *132*, 8935–8944.
(4) Prytkova, T. R.; Kurnikov, I. V.; Beratan, D. N. *Science* **2007**, *315*, 622–625.
(5) Debler, E. W.; Kaufmann, G. F.; Meijler, M. M.; Heine, A.; Mee, J. M.; Pljevaljcic, G.; Di Bilio, A. J.; Schultz, P. G.; Millar, D. P.; Janda, K. D.; Wilson, I. A.; Gray, H. B.; Lerner, R. A. *Science* **2008**, *319*, 1232–1235.
(6) Weber, S.; Biskup, T.; Okafuji, A.; Marino, A. R.; Berthold, T.; Link, G.; Hitomi, K.; Getzoff, E. D.; Schleicher, E.; Norris, J. R. *J. Phys. Chem. B* **2010**, *114*, 14745–14754.
(7) Gray, H. B.; Winkler, J. R. *Biochim. Biophys. Acta-Bioenerg.* **2010**, *1797*, 1563–1572.
(8) Wang, H. Y.; Lin, S.; Allen, J. P.; Williams, J. C.; Blankert, S.; Laser, C.; Woodbury, N. W. *Science* **2007**, *316*, 747–750.
(9) Lin, J. P.; Balabin, I. A.; Beratan, D. N. *Science* **2005**, *310*, 1311–1313.
(10) Balabin, I. A.; Onuchic, J. N. *Science* **2000**, *290*, 114–117.
(11) van der Est, A.; Prisner, T.; Bittl, R.; Fromme, P.; Lubitz, W.; Mobius, K.; Stehlik, D. *J. Phys. Chem. B* **1997**, *101*, 1437–1443.
(12) Weber, S. *Biochim. Biophys. Acta-Bioenerg.* **2005**, *1707*, 1–23.
(13) Kim, S. T.; Sancar, A.; Essenmacher, C.; Babcock, G. T. *Proc. Natl. Acad. Sci. U.S.A.* **1993**, *90*, 8023–8027.
(14) Shih, C.; Museth, A. K.; Abrahamsson, M.; Blanco-Rodriguez, A. M.; Di Bilio, A. J.; Sudhamsu, J.; Crane, B. R.; Ronayne, K. L.; Towrie, M.; Vlček, A., Jr.; Richards, J. H.; Winkler, J. R.; Gray, H. B. *Science* **2008**, *320*, 1760–1762.
(15) Dempsey, J. L.; Winkler, J. R.; Gray, H. B. *Chem. Rev.* **2010**, *110*, 7024–7039.
(16) Komatsu, T.; Wang, R.-M.; Zunszain, P. A.; Curry, S.; Tsuchida, E. *J. Am. Chem. Soc.* **2006**, *128*, 16297–16301.
(17) Woolerton, T. W.; Sheard, S.; Pierce, E.; Ragsdale, S. W.; Armstrong, F. A. *Energy Environ. Sci.* **2011**, *4*, 2393–2399.
(18) Hasegawa, J.; Nakatsuji, H. *Chem. Lett.* **2005**, *34*, 1242–1243.
(19) McConnel, H. *J. Chem. Phys.* **1961**, *35*, 508–515.
(20) Hasegawa, J.; Nakatsuji, H. *J. Phys. Chem. B* **1998**, *102*, 10420–10430.
(21) Kobori, Y.; Norris, J. R. *J. Am. Chem. Soc.* **2006**, *128*, 4–5.
(22) Kobori, Y.; Fuki, M.; Murai, H. *J. Phys. Chem. B* **2010**, *114*, 14621–14630.
(23) Park, J. S.; Karnas, E.; Ohkubo, K.; Chen, P.; Kadish, K. M.; Fukuzumi, S.; Bielawski, C. W.; Hudnall, T. W.; Lynch, V. M.; Sessler, J. L. *Science* **2010**, *329*, 1324–1327.
(24) Kobori, Y.; Shibano, Y.; Endo, T.; Tsuji, H.; Murai, H.; Tamao, K. *J. Am. Chem. Soc.* **2009**, *131*, 1624–1625.
(25) Atkins, P. W.; Evans, G. T. *Mol. Phys.* **1974**, *27*, 1633–1644.
(26) Murai, H.; Hayashi, T.; Ihaya, Y. J. *Chem. Phys. Lett.* **1984**, *106*, 139–142.
(27) Akiyama, K.; Tero-Kubota, S.; Ikoma, T.; Ikegami, Y. *J. Am. Chem. Soc.* **1994**, *116*, 5324–5327.
(28) Da Ros, T.; Prato, M.; Guldi, D. M.; Ruzzi, M.; Pasimeni, L. *Chem.—Eur. J.* **2001**, *7*, 816–827.
(29) Lebedeva, N. V.; Tarasov, V. F.; Resendiz, M. J. E.; Garcia-Garibay, M. A.; White, R. C.; Forbes, M. D. E. *J. Am. Chem. Soc.* **2010**, *132*, 82–84.
(30) Bosch, M. K.; Proskuryakov, I. L.; Gast, P.; Hoff, A. J. *J. Phys. Chem.* **1995**, *99*, 15310–15316.
(31) Ghuman, J.; Zunszain, P. A.; Petitpas, I.; Bhattacharya, A. A.; Otagiri, M.; Curry, S. *J. Mol. Biol.* **2005**, *353*, 38–52.
(32) Huvaere, K.; Skibsted, L. H. *J. Am. Chem. Soc.* **2009**, *131*, 8049–8060.
(33) Loeff, I.; Rabani, J.; Treinin, A.; Linschitz, H. *J. Am. Chem. Soc.* **1993**, *115*, 8933–8942.
(34) Thielges, M.; Uyeda, G.; Camara-Artigas, A.; Kalman, L.; Williams, J. C.; Allen, J. P. *Biochemistry* **2005**, *44*, 7389–7394.
(35) McGlynn, S. P.; Azumi, T.; Kinoshita, M. *Molecular Spectroscopy of the Triplet State*; Prentice Hall: Englewood Cliffs, NJ, 1969.
(36) Closs, G. L.; Forbes, M. D. E.; Norris, J. R. *J. Phys. Chem.* **1987**, *91*, 3592–3599.
(37) Buckley, C. D.; Hunter, D. A.; Hore, P. J.; McLauchlan, K. A. *Chem. Phys. Lett.* **1987**, *135*, 307–312.
(38) Anderson, P. W. *Phys. Rev.* **1959**, *115*, 2–13.
(39) Kobori, Y.; Sekiguchi, S.; Akiyama, K.; Tero-Kubota, S. *J. Phys. Chem. A* **1999**, *103*, 5416–5424.
(40) Kobori, Y.; Yamauchi, S.; Akiyama, K.; Tero-Kubota, S.; Imahori, H.; Fukuzumi, S.; Norris, J. R. *Proc. Natl. Acad. Sci. U.S.A.* **2005**, *102*, 10017–10022.
(41) Scott, A. M.; Miura, T.; Ricks, A. B.; Dance, Z. E. X.; Giacobbe, E. M.; Colvin, M. T.; Wasielewski, M. R. *J. Am. Chem. Soc.* **2009**, *131*, 17655–17666.
(42) Bixon, M.; Jortner, J.; Michel-Beyerle, M. E. *Chem. Phys.* **1995**, *197*, 389–404.
(43) Tanaka, S.; Marcus, R. A. *J. Phys. Chem. B* **1997**, *101*, 5031–5045.
(44) Kamal, J. K. A.; Zhao, L.; Zewail, A. H. *Proc. Natl. Acad. Sci. U.S.A.* **2004**, *101*, 13411–13416.
(45) Fukuzumi, S. *Phys. Chem. Chem. Phys.* **2008**, *10*, 2283–2297.